Title: Genetic ablation of the DNA demethylation pathway in retinal progenitor cells impairs photoreceptor development and function, leading to retinal dystrophy

Galina Dvoriantchikova[1], Chloe Moulin[1], Michelle Fleishaker[1], Vania Almeida[2], Daniel Pelaez[1], Byron L. Lam[1], Dmitry Ivanov[1,3*]

[1]Bascom Palmer Eye Institute, Department of Ophthalmology, University of Miami Miller School of Medicine, Miami, FL, 33136, USA
[2]The Miami Project to Cure Paralysis, University of Miami Miller School of Medicine, FL, 33136, USA
[3]Department of Microbiology and Immunology, University of Miami Miller School of Medicine, Miami, FL, 33136, USA

*corresponding author

Correspondence: Dr. Dmitry Ivanov, Bascom Palmer Eye Institute, Department of Ophthalmology, University of Miami Miller School of Medicine, 1638 NW 10th Ave, Miami, FL 33136, USA, Tel 305-482-4230, Fax 305-547-3718. E-mail: divanov@med.miami.edu.

Abstract
Rod and cone photoreceptors are critical for vision, and their loss leads to blindness. We explored the role of epigenetic mechanisms in photoreceptor development and function that is still poorly understood. To this end, we created mice in which the DNA demethylation pathway was inactivated in retinal progenitor cells (RPCs). We have shown that DNA demethylation caused by the activity of TET oxidases is necessary during the differentiation of RPCs into photoreceptors. Disruption of the TET-dependent DNA demethylation pathway prevents the proper expression of genes necessary for photoreceptor development and function (e.g., *Rho, Nr2e3, Prph2, Pde6a, Pde6b, Pde6g, Cplx4, Grk1, Cnga1, Cngb1, Cplx4*). The result of this is underdevelopment or complete absence of outer segments and synaptic termini in photoreceptors of TET-deficient retinas, resulting in loss of rod and cone function, as assayed by electroretinogram. The number of photoreceptors decreases in the TET-deficient retinas over time, leading to retinal dystrophy.

Main

Retinal rod and cone photoreceptors convert light into electrical signals, which, upon traveling to the brain, create the sensation of vision [1, 2]. The loss of these neurons results in blindness. There are many signaling cascades that regulate the differentiation of photoreceptors from retinal progenitor cells (RPCs) and their subsequent maturation into functional neurons [3, 4]. Impaired activity of these signaling cascades as a result of inherited mutations in the corresponding genes leads to various retinal dystrophies, such as retinitis pigmentosa, cone and cone-rod dystrophy, congenital stationary night blindness, and Leber congenital amaurosis [5-7]. However, are genetic mechanisms the only ones that can influence the activity of these signaling cascades?

DNA methylation is an epigenetic mechanism that is responsible for modifying cytosines into 5-methylcytosines [8, 9]. DNA methylation in regulatory elements (e.g., promoters, enhancers) leads to reduced expression of the corresponding genes, while DNA demethylation should occur to promote the gene expression [8-11]. Photoreceptors are a unique cell type from an epigenetic perspective, as the promoters of many genes critical for the development and function of these neurons are highly methylated (hypermethylated) in human and murine RPCs (e.g., *Nr2e3, Rho, Prph2, Pde6a, Pde6b, Pde6g, Rcvrn, Cnga1, Grk1, Cplx4*) [12, 13]. Some of these promoters were still hypermethylated in DNA isolated from rod precursors [14]. Meanwhile, the methylation levels of the promoters of genes essential for photoreceptor development and function were low, and the expression of these genes was high in mature photoreceptors [12-14]. Hence, there must be a mechanism that would lead to demethylation of the promoters of these genes during the differentiation of RPCs into photoreceptors. The observed anticorrelation between the levels of gene expression and the levels of methylation of their promoters does not yet guarantee that the pathway responsible for DNA demethylation plays an important role in the development and function of photoreceptors. However, if the role of this pathway is significant, then disruption of its activity should prevent the development and function of photoreceptors, leading to retinal pathologies. An important indication of the possible significance of the DNA demethylation pathway is that many genes whose promoters were highly methylated in RPCs are involved in various forms of retinal dystrophies [5-7].

The patterns of methylated cytosines in DNA are established by the methyltransferase (DNMT) family of enzymes that catalyze the transfer of a methyl group to the 5th position in the cytosine nucleotide [8, 9]. Meanwhile, the Ten-Eleven Translocation (TET) family of 5-methylcytosine oxidases is responsible for DNA demethylation, which occurs in several steps with the participation of additional signaling cascades and ends with the appearance of unmodified cytosines [10, 11]. In this study, we examined how inactivation of the TET-dependent DNA demethylation pathway in RPCs affects the development and function of photoreceptors. We found that genetic ablation of the TET-dependent DNA demethylation pathway in RPCs prevents demethylation of the promoters of key genes essential for photoreceptor development and function (e.g., *Nr2e3, Rho, Prph2, Pde6a, Pde6b, Pde6g, Rcvrn, Cnga1, Grk1, Cplx4*). This, in turn, significantly reduces their expression, preventing the development of photoreceptor outer segments and synapses. Such underdeveloped photoreceptors are deprived of function and die over time. These findings suggest the contribution of retina-specific epigenetic mechanisms to the pathogenesis of retinal dystrophies.

Results

Genetic ablation of the TET family in RPCs prevents photoreceptor development

The TET family, comprising of the *Tet1*, *Tet2*, and *Tet3* genes, is highly expressed at all stages of retinal development, including the earliest stage when the retina consists mostly of RPCs (**Fig. 1A**, **1B**) [15]. To study the role of the TET-dependent DNA demethylation pathway in photoreceptor development and function, we used transgenic animals in which the exons encoding Tet1, Tet2, and Tet3 enzymatic domains were flanked by loxP sites (**Fig. 1C**) [16, 17]. These animals were crossed to produce triple Tet1/Tet2/Tet3-floxed animals (TET, **Fig. 1D**). To inactivate the TET family in RPCs, we used Chx10-cre mice (Chx10/Vsx2 is a marker of RPCs) that were created about 20 years ago and have been used extensively by many investigators to this day to study retinal development (**Fig. 1D**) [18]. It was shown that Chx10-cre-expressing RPCs differentiate into all types of retinal cells including rod and cone

photoreceptors [18]. We found that there were no significant morphological and functional differences between TET and Chx10-cre animals (**Fig. 1E-1I**). Meanwhile, when we crossed TET and Chx10-cre to produce Chx10-TET mice in which the RPCs lacked the activity of TET enzymes due to cre-mediated excision of TET catalytic domains, we found significant changes in the structure and function of the photoreceptors. While the size of TET eyeballs was relatively smaller than those of Chx10-cre, the size of the eyeballs of the Chx10-TET mice was significantly smaller than those of TET and Chx10-cre (**Fig. 1E**). The retinas of Chx10-TET mice had virtually no outer segments (OS) and outer plexiform layers (OPL) (**Fig. 1F**). The absence of OPL resulted in the cells of the outer nuclear layer (ONL) and the inner nuclear layer (INL) mixing (**Fig. 1F**). Electroretinogram (ERG) tests conducted on dark-adapted (rod) animals showed ten times less Chx10-TET rod photoreceptor activity compared to TET and Chx10-cre (b-wave [mean±sem uV]: TET 266±14 vs. Chx10-cre 256±14 vs. Chx10-TET 21±4; a-wave: TET -123±11 vs. Chx10-cre -104±7 vs. Chx10-TET -17±3; n=10-20 eyes tested); the Chx10-TET ERG traces were almost flat (**Fig. 1G**). Similar results were obtained in the light-adapted (cone) animals (b-wave [mean±sem uV]: TET 50±3 vs. Chx10-cre 53±6 vs. Chx10-TET 14±2; flicker: TET 35±2 vs. Chx10-cre 28±3 vs. Chx10-TET 6±1; **Fig. 1H, 1I**). All these data indicate that, unlike TET and Chx10-cre animals, Chx10-TET mice were functionally blind.

TET-deficient photoreceptors lack OS and synaptic termini, which prevents them from functioning normally, leading to retinal dystrophy

We then undertook more detailed studies of Chx10-TET and TET animals since Chx10-cre animals were previously well studied and did not differ much from TET mice. To this end, we collected retinas from animals of different ages to investigate the thickness of their layers. The thickness was measured every 200 µm starting from the optic nerve head and then this thickness was averaged (**Fig. 2A, 2B, Supplementary Fig. S1, S2**). We found that the OS and OPL were poorly developed or absent already in the retinas of very young Chx10-TET animals (postnatal-day [P] 14), while OS and OPL of TET animals were well-developed (**Fig. 2A, 2B**). A more detailed analysis of our IHC data indicates the presence of underdeveloped OS of cones in P14 and 1-month-old Chx10-TET mice, but their absence in 3- and 6-month-old Chx10-TET animals (the conclusion was made based on staining with PNA, which is a marker of cone OS; **Fig. 2A, 2B**). The OS of the rods are absent in Chx10-TET mice of all ages (**Fig. 2A, 2B**). We found some differences in the thickness of the ONL in P14 and one-month-old (1m) Chx10-TET compared to TET mice. However, these differences began to become more significant with age, reaching as few as three lines of nuclei in some parts of the ONL of 6-month-old Chx10-TET animals (P14 TET vs Chx10-TET, µm: 58±2 vs. 51±2; 1m TET vs Chx10-TET, µm: 57±2 vs. 42±2; 3m TET vs Chx10-TET, µm: 52±2 vs. 32±1; 6m TET vs Chx10-TET, µm: 47±1 vs. 21±1; **Fig. 2A, 2B, Supplementary Fig. S2**). Thus, photoreceptor developmental disorders lead to their eventual death. However, we found only a few dead cells in 3-month-old Chx10-TET retinas using TUNEL assay (**Supplementary Fig. S3**). These findings suggest that few cells die over a given period of time in Chx10-TET retinas and surrounding cells manage to successfully phagocytose the dead cells. For this reason, we can only detect a small number of dead cells using TUNEL assay. These results are consistent with the slow retinal degeneration we observed in Chx10-TET mice (**Fig. 2A, 2B**). It should be also noted that we did not find significant changes in the thickness of the INL and inner plexiform layer (IPL) in the retinas of Chx10-TET and TET mice of all ages (**Fig. 2A, 2B, Supplementary Fig. S2**). We found that the size of the retinas of Chx10-TET mice is smaller than in TET mice (**Fig. 2B, Supplementary Fig. S1**). These observations are consistent with the fact that Chx10-TET mice have smaller eyeballs than TET mice (**Fig. 1E**).

To study in detail the morphology of TET-deficient photoreceptors, we used transmission electron microscopy (TEM). TEM examination revealed well-developed OS in the photoreceptors of TET animals (**Fig. 2C, Supplementary Fig. S4**). Meanwhile, the OS were undeveloped or completely absent in the photoreceptors of TET-deficient (Chx10-TET) 1-month-old animals (**Fig. 2C, Supplementary Fig. S4**). We found a clear separation in TET retinas of the ONL from the INL by the OPL in which photoreceptor synapses were present. At the same time, the cells of the ONL and INL were mixed in the retinas of the Chx10-TET mice; synapses are difficult to find in these retinas (**Fig. 2D-2D", Supplementary Fig. S4**).

Our data also suggest that chromatin in the nuclei of the ONL of Chx10-TET animals was less condensed compared to TET mice (**Fig. 2E**). All these abnormalities in the structure of TET-deficient photoreceptors led to the fact that even 1-month-old animals were already functionally blind according to ERG tests (**Supplementary Fig. S5**). We would also like to note that Chx10-cre animals exhibit mosaicism in the expression of cre recombinase in RPCs, which leads to the fact that the effect of TET inactivation can be stronger or weaker in different parts of the retina [18]. We found this effect during TEM examination. While in most Chx10-TET retinas the OS and synapses were poorly developed or absent, small areas could be found where the OS and synapses were well developed (**Supplementary Fig. S4**). This could explain the presence of weak photoreceptor activity in Chx10-TET animals assayed by ERG.

Genetic ablation of the TET family has less impact on the development of non-photoreceptors in the retina

We also assessed in our study the effect of inactivation of the TET-dependent DNA demethylation pathway on other retinal cell types. In addition to significant changes in photoreceptor morphology, we found some changes in Muller glia morphology (**Fig. 3A-3D**). We also found that expression of a Muller glia marker Glul was decreased using western blot analysis (**Fig. 3E**). We did not detect significant changes associated with bipolar, amacrine, and horizontal cells (**Fig. 3C, 3F**). However, synaptic contacts in the IPL were less structured in Chx10-TET retinas (**Fig. 3F-3F"**). We also measured the thickness of the animals' optic nerve at 0.5 mm, 2 mm, and 3.5 mm from the globe, and then averaged these values. We found that the optic nerves in the Chx10-TET mice were thinner than in TET mice (260±6 µm vs. 357±5 µm, P value < 0.0001, n=10-12 optic nerves; **Fig. 3G**). Since the axons of RGCs form the optic nerve, we analyzed the density of these neurons in the ganglion cell layer (GCL). We did not find differences in the density of RGC in the GCL of TET and Chx10-TET animals (**Fig. 3B, 3H**). We assume that a smaller retinal size with the same density of RGCs leads to a smaller total number of RGCs and, as a result, a smaller number of axons and, accordingly, a smaller thickness of the Chx10-TET optic nerves.

Expression of genes required for photoreceptor development and function is significantly reduced in TET-deficient retinas

Photoreceptor developmental disorders upon inactivation of the TET-dependent DNA demethylation pathway should be reflected in the expression of the corresponding genes. To this end, we investigated gene expression in the retinas of Chx10-TET and TET animals using RNA-seq analysis. Since photoreceptors make up 70-80% of all cells in the retina, by studying the gene expression of the whole retina we are actually studying the gene expression of the photoreceptors [19]. The retinas were collected at P14 and one month (1m) and used for preparation of RNA-seq libraries for next-generation sequencing (NGS; P14, n = 3; 1m, n=4). We chose P14 and 1m animals because the ONL containing photoreceptors differ slightly between Chx10-TET and TET mice at these ages. Our RNA-seq data indicated that gene expression in Chx10-TET retinas is significantly changed compared to that in TET retinas. This difference is clearly seen from the sample clustering, principal component analysis, and volcano plots (**Fig. 4A-4C, Supplementary Data S1**). We were somewhat surprised by the lack of difference in the expression of *Tet1*, *Tet2*, and *Tet3*. However, when we considered the expression of only those TET transcripts in which exons encoding catalytic domains are retained, we found a significant decrease in the expression of these genes (**Supplementary Fig. S6**). These results indicate the stability of the *Tet1*, *Tet2*, and *Tet3* transcripts even in the absence of several exons in them. We used k-means clustering to identify coherently expressed groups of genes. We found that the cluster in which TET vs. Chx10-TET gene expression is reduced includes a large number of genes responsible for the development and function of photoreceptors (**Fig. 4D**). Overall, our results indicate that the expression of genes required for phototransduction, as well as OS, inner segment, cilium, and synapse development and function was significantly reduced in Chx10-TET retinas compared to TET (**Fig. 4E, 4F, Supplementary Data S1**). These genes include *Rho*, *Pde6a*, *Pde6b*, *Pde6g*, *Gnat1*, *Rcvrn*, *Grk1*, *Prph2*, *Guca1b*, *Slc24a1*, *Cnga1*, *Cplx4*, *Unc119*, *Ush2a* (**Fig. 4E, 4F**). These results explain the morphological changes we observed in Chx10-TET photoreceptors (**Figs. 1** and **2**). We found significantly reduced expression of 56 genes, each of which leads to a form of either retinitis pigmentosa, cone or cone-rod dystrophy, congenital

stationary night blindness, or Leber congenital amaurosis (**Fig. 4G, Supplementary Data S1**). Our RNA-seq data were in agreement with the results of western blot analysis: Nr2e3, Rho, Pde6a, Pde6b, Prph2, Rcvrn proteins were virtually undetectable in Chx10-TET retinas (**Fig. 4H**). Our results also indicate that most of the genes whose expression was decreased are critical for rod photoreceptor development and function (**Fig. 4F, Supplementary Data S1**). At the same time, the expression of some genes necessary for cone photoreceptor function was increased (e.g., *Opn1sw*, *Pde6c*, *Gnat2*, *Gngt2*, *Arr3*, *Slc24a*, *Cnga3*, *Cngb3*, **Fig. 4F, Supplementary Data S1**). These results can be explained by the fact that the expression of *Nrl*, *Nr2e3*, *Esrrb*, and *Samd7* transcription factors essential for rod development and function was significantly reduced (**Fig. 4F, Supplementary Data S1**). Thus, the TET-dependent DNA demethylation pathway may play a more important role in the development and function of rods than cones. However, reduced expression of genes (e.g., *Prph2, Rom1, Slc24a1, Rcvrn, Mpp4, Cplx4*) important for the function of both types of photoreceptors leads to the negative impact of inactivation of this pathway on both rods and cones. We also found reduced expression of *Pde6h* and *Opn1mw* cone-related genes.

Genetic ablation of the TET family prevents demethylation of the promoters of genes essential for photoreceptor development and function during the differentiation of RPCs into rods and cones

The entirety of our data indirectly indicates that the level of methylation of genes necessary for the development and function of photoreceptors should remain high in retinas in which the TET-dependent DNA demethylation pathway is inactive (Chx10-TET mice). Meanwhile, this level of methylation should be reduced in retinas where the activity of this pathway was not impaired (TET mice). To directly examine methylation levels in retinas of Chx10-TET and TET animals, we used whole genome bisulfite sequencing (WGBS). We used whole P14 retinas in our study because 70-80% of the cells in them are photoreceptors [19]. Thus, changes in methylation of photoreceptor gene promoters can be easily detected. To this end, we isolated DNA from retinas of three P14 Chx10-TET mice and three P14 TET animals. These DNA samples were used in the preparation of six WGBS libraries for NGS. To analyze our NGS data, we used methylKit Bioconductor R package [20]. The CpG methylation clustering and principal component analysis indicate a clear difference between the methylation patterns in DNA isolated from the retinas of Chx10-TET vs. TET mice (**Fig. 5A, 5B, Supplementary Data S2**). By combining the capabilities of methylKit and annotatr Bioconductor R packages, we created a list of genes in which all promoters and first exons were highly methylated (hypermethylated) in the retinas of Chx10-TET animals; methylation of at least one promoter or the first exon should be low in the retinas of TET mice (**Supplementary Data S2**) [20, 21]. We used this list to analyze the biological processes and diseases in which these genes are involved. We also investigated what cellular components the proteins encoded by these genes might be part of. A significant number of genes we found are involved in the development and function of photoreceptors (e.g., *Rho, Prph2, Rcvrn, Pde6g, Pde6a, Pde6b, Nr2e3, Cnga1, Cngb1, Grk1, Cplx4, Ush2a, Aipl1, Nxnl1,* **Fig. 5C-5E, Supplementary Data S2**). Virtually all diseases are various forms of retinal dystrophies (**Fig. 5D**). Analysis of the methylation and expression levels of these genes showed that high levels of methylation are associated with low levels of expression of these genes in Chx10-TET animals (**Fig. 5E**). Conversely, low methylation levels are associated with high expression levels of these genes in TET mice (**Fig. 5E**). We also found significant changes in mean methylation levels and methylation of individual cytosines in Chx10-TET vs. TET mice at locations close to the transcription start sites (TSS) of studied genes (**Fig. 5F, Supplementary Fig. S7**). These results suggest that high levels of cytosine methylation in TSS may interfere with the efficient initiation of transcription of genes necessary for photoreceptor development and function, causing retinal abnormalities. Our results also indicate that a significant number of genes whose promoters remain highly methylated in Chx10-TET mouse retinas are important for rod development and function (e.g., *Nr2e3, Rho, Pde6a, Pde6b, Pde6g, Cnga1, Grk1*). Of particular note, there is a high level of methylation of *Nr2e3* transcription factor, without which the proper development of rods is not possible [3, 4]. However, high methylation levels of the promoters of genes that are important for function of both photoreceptor types (e.g., *Prph2, Rcvrn, Cplx4*) should have an impact on the function of cones in Chx10-TET mice.

Discussion

Disturbances in the development and function of photoreceptors invariably lead to blindness, which can have devastating consequences on a person's normal life [5-7]. Understanding the mechanisms responsible for the development and function of photoreceptors allows us to restore visual function by imparting activity to abnormal photoreceptors or via the regeneration of lost photoreceptors. While significant progress has been made in understanding the signaling cascades that regulate photoreceptor development and function, the contribution of epigenetic mechanisms to these processes is poorly understood [3, 4, 9]. The objective of this study was to explore the role of the TET-dependent DNA demethylation pathway in photoreceptor development and function. We found that genetic ablation of the TET family prevents the DNA demethylation process during the differentiation of RPCs into photoreceptors. Preservation of methylated cytosines in the promoters of genes necessary for the development and function of photoreceptors leads to significantly reduced expression of the corresponding genes. All these events interfere with the development of photoreceptor OS and synapses, depriving the retina of functioning rod and cone photoreceptors. Over time, the number of photoreceptors decreases in TET-deficient retinas, leading to retinal dystrophy.

The differentiation of RPCs into photoreceptors includes a specification stage when the photoreceptor precursors decide whether they will be rods or cones, and a maturation stage when the OS, synapses, and other components of the photoreceptors necessary for their function are formed [3, 4]. Otx2 and Crx transcription factors are necessary for RPCs to adopt the fate of photoreceptor precursors [3, 4]. Onecut1 and Onecut2, in turn, are responsible for cone specification in the presence of Crx [3, 4, 22-24]. Meanwhile, Nrl, Nr2e3, and Crx are responsible for rod specification [3, 4, 22-24]. Our data suggest that DNA methylation does not affect the activity of Crx, Onecut1, and Onecut2 and thus does not interfere with cone specification (**Supplementary Data S1 and S2**). We also found increased expression of genes essential for cone maturation in Chx10-TET vs. TET retinas (**Fig. 4F**). At the same time, the expression of almost all genes necessary for rod specification and maturation was reduced in Chx10-TET vs. TET retinas (**Fig. 4F**). The promoters of genes such as *Nr2e3, Samd7, Rho, Pde6a, Pde6b, Pde6g, Prph2, Cplx4, Grk1, Cnga1, Rcvrn* remained highly methylated (hypermethylated) and weakly active in the retinas of P14 Chx10-TET animals (**Supplementary Data S1 and S2**). All these results indicate that DNA methylation, as an epigenetic mechanism, regulates the specification and maturation of rod photoreceptors, possibly preventing their appearance at an early stage of retinal development. However, the fact that some genes that must be demethylated during RPC differentiation into photoreceptors are used by cones and rods leads to inevitable issues during cone maturation. We also found that the expression of *Opn1mw* and *Pde6h* required for cone maturation was reduced in the retinas of Chx10-TET mice. Thus, the TET-dependent DNA demethylation pathway contributes to cone maturation.

Disruption of the activity of the TET-dependent DNA demethylation pathway leads to reduced expression of many genes, mutations of which lead to one or more forms of either retinitis pigmentosa, cone and cone-rod dystrophy, congenital stationary night blindness, or Leber congenital amaurosis (**Fig. 4G, Supplementary Data S1**). Thus, it is not surprising that we observed such serious disturbances in the development and function of TET-deficient photoreceptors leading to their death. However, mutations in either TET1, TET2, or TET3 leading to retinal dystrophies have not been detected, possibly due to the functional redundancy of these genes [10, 11, 16, 17]. Meanwhile, global knockout of all three genes is lethal for embryos [25]. Could any retinal dystrophy forms be caused by disturbances in the process of DNA demethylation then? TET enzymes need partners (transcription factors with a DNA binding domain) to bind to highly methylated (hypermethylated) DNA and to initiate targeted DNA demethylation [26-32]. If there are no such transcription factors or their activity is impaired, then the DNA demethylation process cannot be started even in the presence of TET enzymes. Mutations in transcription factors that prevent TET enzymes from binding to promoters can prevent demethylation of one or more genes necessary for the development and function of photoreceptors (e.g., *Nr2e3, Rho, Pde6a, Pde6b, Pde6g, Prph2, Grk1, Cnga1, Cngb1, Nxnl1, Ush2a*), leading to a form of retinal dystrophy. Phenotypically, it may be similar to the form caused by mutations, but this time this form of retinal dystrophy will be caused by epigenetic

mechanisms. Hard work lies ahead to identify partners of TET enzymes that promote demethylation of genes necessary for the development and function of photoreceptors.

Finally, we have shown in our study that disruption of the activity of the TET-dependent DNA demethylation pathway in RPCs impairs the development and function of photoreceptors, leading to retinal dystrophy. While the TET-dependent DNA demethylation pathway affects the development of both types of photoreceptors, we found a stronger impact of this pathway on the development of rods than cones. Given that rods are necessary for the survival of cones, even a lesser influence of the TET-dependent DNA demethylation pathway on cone development and function will still inevitably lead to cone death [33]. However, slow death of undeveloped photoreceptors (significant retinal degeneration was observed in 6-month-old Chx10-TET animals) creates a window of opportunity to remove methylation and trigger the development of these neurons, restoring their function. Thus, the contribution of retina-specific epigenetic mechanisms to the pathogenesis of retinal dystrophies may significantly change current approaches to diagnosing and treating these diseases.

Methods

Generation of TET conditional knockouts and genotype analysis

All procedures were executed in compliance with the National Institutes of Health (NIH) Guide for the Care and Use of Laboratory Animals and according to the University of Miami Institutional Animal Care and Use Committee (IACUC) approved protocol (Protocol #: 23-058). To generate TET triple floxed animals, we crossbred Tet1-floxed, Tet2-floxed, and Tet3-floxed animals (these animals are gifts from Dr. Anjana Rao, La Jolla Institute for Immunology). TET mice served as controls. To genotype TET animals, we used primers: a) Tet1 floxed: F: CAG TTC TAT TCA GTA AGT AAG TGT GCC, R: GGT TGT GTT AAA GTG AGT TGC AAG CG (WT/WT – will have 1 band of 198bp, FL/WT – will have 2 bands [198bp and 242bp], FL/FL – will have 1 band of 242bp); b) Tet2 floxed: F: GCC CAA GAA AGC CAA GAC CAA GAA, R: AAG GAG GGG ACT TTT ACC TCT CAG AGC AA (WT/WT – will have 1 band of 650bp, FL/WT – will have 2 bands [650bp and 780bp], FL/FL – will have 1 band of 780bp); c) Tet3 floxed: F: GGA TGT GAG CTA GTT CTC CTA ACT TGA GAG G, R: CCC TGT CTA CTC TAT TCT TGT GTC AGG AGG (WT/WT – will have 1 band of 195 bp, FL/WT – will have 2 bands [195 bp and 349 bp], FL/FL – will have 1 band of 349bp). We selected only floxed alleles. To inactivate TET enzymes in RPCs, we used Chx10-cre mice (strain #:005105, the Jackson Laboratory). To generate triple conditional Chx10-TET knockout animals, we crossed Chx10-cre and TET mice. To genotype Chx10-TET animals, we used TET primers above and primers to detect cre transgene (F: GCG GTC TGG CAG TAA AAA CTA TC, R: GTG AAA CAG CAT TGC TGT CAC TT). Subsequently, we crossed Chx10-TET and TET mice in order to obtain Chx10-TET and TET littermates. We used male and female mice to address sex as a biological variable. Animals were housed under standard conditions. They were given free access to food and water and had a 12-hour light to dark cycle. All methods were completed and reported in accordance with ARRIVE guidelines.

Electroretinogram (ERG) tests

Prior to scotopic ERG recording, mice were dark-adapted for more than 8 hours with free access to food and water. For photopic ERG recordings, mice were adapted to background white light for 10 minutes. For all ERG tests pupils were dilated with 1% tropicamide for 5 minutes. Mice were anesthetized with 80 mg/kg of ketamine and 10 mg/kg of xylazine delivered IP and positioned dorsally in a headholder. The body temperature was kept at 37±0.5°C with a temperature-controlled heating pad. Animals were screened for cataracts or corneal opacities. The Celeris electrodes were lubricated with Systane gel (0.3% Hypromellose) (Alcon, Geneva, Switzerland) prior to placement on the corneas of each animal. The dual function stimulator-electrodes deliver a light stimulus and record neural electrical activity simultaneously. ERG recordings were collected using the Celeris D430 rodent ERG testing system (Diagnosys LLC, MA) paired with the Espion software (V6.64.14; Diagnosys LLC) following the manufacturer's protocols. Briefly, both eyes of animals were exposed to a series of single white-light flashes. Scotopic tests subjected dark-adapted animals to intensities of 0.01, 0.1, and 1.0 cd.s/m² at a frequency of 1.00 Hz. B-

wave amplitudes were measured from the trough of the a-wave to the peak of the subsequent b-wave. The a-wave's negative trough was analyzed at an intensity of 1.0 cd.s/m². For photopic ERGs, light-adapted animals were given flash stimuli of 3 and 10 cd.s/m². Both scotopic and photopic ERG recordings were sampled at a frequency of 2000 Hz, covering a duration from 50 ms before to 300 ms after the stimulus. Flicker ERG was performed using continuous 6500K white light flashes with an intensity of 3 cd.s/m² at 10 or 30 Hz, against a background of 30 cd/m² 6500K white light. Data for Flicker ERG was acquired at a sample frequency of 2000 Hz, spanning from 10 ms before to 250 ms after the stimulus. Oscillatory potentials were automatically isolated and measured from the ascending limb of the b-wave using Espion software, which also computed all amplitudes. Each trace marker was reviewed, and any errors were manually corrected.

Necropsy and tissue collection

To collect eyeballs, retinas, and optic nerves, the mice were injected IP with ketamine (80 mg/kg) and xylazine (10 mg/kg). When we confirmed that the animals were under deep anesthesia, we opened the chest cavity and placed a syringe needle into the heart. The syringe needle was attached to a pump to allow phosphate buffered saline (PBS, pH 7.4; #10010023, ThermoFisher Scientific) to circulate through the animal. Eyeballs and optic nerves were then carefully dissected out, taking care not to apply any pressure on them that could influence the results of morphological analysis and other experiments. Optic nerves were dissected from their insertion point behind the globe all the way to the optic chiasm. The size of the eyeballs and optic nerves were determined on Nikon SMZ1270 stereo microscope using Micrometrics SE Premium software. The retinas removed from the eyes were collected in the appropriate buffers for RNA and DNA purification, transmission electron microscopy (TEM), immunohistochemistry, and western blot analysis.

Study of the thickness of the Chx10-TET and TET retinal layers

The eyeballs were fixed with 4% paraformaldehyde (PFA, in PBS), and then, were placed in 30% sucrose (in PBS) for cryoprotection overnight. The next day, the eyeballs were embedded into Cryo-Gel (Leica), frozen in a −80°C freezer, and then, sectioned on a Leica cryostat at 12 µm. We collected only those retinal sections that contained the optic nerve head. The retinal sections were permeabilized with 0.3% Triton X-100 in PBS, washed with PBS, and blocked in a buffer containing 5% donkey serum, 2% BSA and 0.15% Tween-20 in PBS. To stain retinal sections, we added an anti-Rho (1:100, PA5-85608, ThermoFisher Scientific) antibody (to label rod outer segments) and peanut lectin (PNA, L32458, ThermoFisher Scientific) from *Arachis hypogaea* (to label cone outer segments) to the blocking buffer overnight. The next day, the retinal sections were washed with PBS and incubated with secondary fluorescent antibodies (ThermoFisher Scientific). Hoechst 33342 (H3570, ThermoFisher Scientific) was used to stain the cell nuclei. Images were collected and analyzed using Leica STELLARIS confocal microscope and its software. We determined the average thickness of each retinal layer every 200 µm starting from the head of the optic nerve. To this end, we determined the area of the retinal layer between the boundaries (e.g., between 400 µm and 600 µm). We then measured the length between the boundaries in the layer (this length could differ from 200 µm since the retina is curved) and divided the area by this length. We considered the resulting value to be the average thickness.

Terminal deoxynucleotidyl transferase (TdT) dUTP Nick-End Labeling (TUNEL) assay

To detect dead cells in the retinas, we used the Click-iT Plus TUNEL Assay Kit (C10617, ThermoFisher Scientific) according to manufacturer's instructions.

Transmission electron microscopy (TEM)

The collected experimental and control retinas were fixed in 2% glutaraldehyde in 0.05 M phosphate buffer and 100 mM sucrose, post-fixed overnight in 1% osmium tetroxide in 0.1 M phosphate buffer, and then dehydrated through a graded alcohol series. Retinas processed in this way were embedded in a mixture of EM-bed/Araldite (Electron Microscopy Sciences). Sections (1 µm thick) were stained with

Richardson's stain for observation under a light microscope. Ultrathin sections (100 nm thick) were cut with a Leica Ultracut-R ultramicrotome and stained with uranyl acetate and lead citrate. The grids were viewed at 80 kV in a JEOL JEM-1400 (JEOL, Tokyo, Japan) transmission electron microscope and images captured with an AMT BioSprint 12 (AMT Imaging Systems, Woburn, Massachusetts) digital camera.

Immunohistochemistry

Retinas fixed with 4% PFA were sectioned (100 μm thick) using Leica vibratome. These sections were permeabilized with 0.3% Triton X-100 in PBS, washed with PBS, and blocked in a buffer (5% donkey serum, 2% BSA and 0.15% Tween-20 in PBS). After one-hour, primary antibodies were added to the retinal sections. For these purposes, we used the following antibodies: anti-Rho (1:100, PA5-85608, ThermoFisher Scientific), anti-Opn1sw (1:200, sc-14363, Santa Cruz Biotechnology), anti-Opn1mw (1:200, anti-Opsin red/green, AB5405, MilliporeSigma), anti-Rbpms (1:400, GTX118619, GeneTex), anti-Chx10 (1:200, AB9016, MilliporeSigma), anti-Rcvrn (1:500, AB5585, MilliporeSigma), anti-Tubb3 (1:400; 802001, BioLegend), anti-Glul (1:200, ab73593, Abcam), anti-ChAT (1:200, AB114P, MilliporeSigma), anti-Calbindin D (1:300, C9848, MilliporeSigma). The retinal sections were incubated overnight with primary antibodies, and then, the next day, they were washed with PBS, and incubated with species-specific secondary fluorescent antibodies (ThermoFisher Scientific). Control sections were incubated without primary antibodies. We used Hoechst 33342 (H3570, ThermoFisher Scientific) to stain the cell nuclei. Images were collected using Leica STELLARIS confocal microscope. To perform immunohistochemistry of flat-mounted retinas, retinas fixed with PFA were permeabilized with 0.5% Triton X-100 in PBS, blocked with 0.5% Triton X-100 containing 10% donkey serum in PBS, and then incubated overnight in a buffer (0.2% Triton X-100, 10% donkey serum in PBS) containing primary antibodies. The next day, the retinas were washed with PBS, incubated with species-specific secondary fluorescent antibodies, and washed again. Retinas were flatmounted, coverslipped, and imaged with Leica STELLARIS confocal microscope.

RNA-seq library preparation, sequencing, and data analysis

Total RNA was isolated from retinas using RNeasy Plus Mini Kit (#74134, Qiagen). We evaluated RNA quality and measured RNA quantity using 2100 Bioanalyzer Instrument (Agilent Technologies), Qubit 4 Fluorometer, and the NanoDrop One spectrophotometer (both from ThermoFisher Scientific). We used RNA samples with a RIN score of 8 or higher. To prepare non-stranded RNA-seq libraries, we used mRNA-seq Lib Prep Kit for Illumina (RK20302, ABclonal) according to manufacturer's instructions. Briefly, poly-T oligo-attached magnetic beads were used to isolate the mRNA from total RNA. After fragmentation, the first strand complementary DNA (cDNA) was produced using random hexamer primers followed by the second strand cDNA synthesis. After end repair, adapter ligation, size selection, amplification, and purification, the RNA-seq libraries were ready for next-generation sequencing (NGS). The RNA-seq libraries were sequenced using 2□×□150 paired end (PE) configuration. The FASTQ files obtained in this study were uploaded to the BioProject database (https://www.ncbi.nlm.nih.gov/bioproject/) and are available under the accession number PRJNA1121391. The STAR RNA-seq aligner, HTseq package, and a basic workflow were applied to calculate how many reads overlap each of the mouse genes [34, 35]. To this end, we used GENCODE M25 (GRCm38.p6) Mus musculus reference genome mm10. The differential gene expression analysis was performed using the edgeR R Bioconductor package [36]. We used the DESeq2 R Bioconductor package to perform the sample clustering and principal component analysis (PCA)[37]. The ViDGER R Bioconductor package and Integrative Genomics Viewer (IGV, https://igv.org/) were applied to visualize the RNA-seq data. We used iDEP (ver. 2.01, http://bioinformatics.sdstate.edu/idep/) for k-means clustering and identification of important signaling cascades and biological processes [38].

Western blot analysis

Each individual retina was placed in 50 µL of T-PER buffer (#78510, ThermoFisher Scientific) supplemented with protease inhibitor. Total protein concentrations were measured using the Micro BCA Protein Assay Kit (#23235, ThermoFisher Scientific). The protein concentration determined for each individual retina varied from 4µg/µL to 5µg/µL. The SDS-PAGE gel (NuPAGE Bis-Tris Mini Protein Gels, 4–12%, NP0323BOX, ThermoFisher Scientific) wells were loaded with the same amount of protein. The protein samples were resolved on the gel and transferred to PVDF transfer membrane (#88585, ThermoFisher Scientific). The membranes (blots) were blocked in TBST buffer (Tris-buffered saline and 0.15% Tween-20) containing 5% nonfat dry milk (#9999, Cell Signaling Technology). The blots were probed overnight with primary antibodies diluted in blocking buffer. We used the following antibodies: anti-Rho (1:1500, PA5-85608, ThermoFisher Scientific), anti-Pde6b (1:500, PA1-722, ThermoFisher Scientific), anti-Glul (1:1000, ab73593, Abcam), anti-Rcvrn (1:3000, AB5585, MilliporeSigma), anti-Prph2 (1:2000, 18109-1-AP, Proteintech), anti-Pde6a (1:1000, A7915, ABclonal), anti-Nr2e3 (1:2000, 14246-1-AP, Proteintech). The next day, the blots were washed with TBST and then incubated with secondary antibody (1:10 000, Amersham Biosciences) diluted in TBST containing 2.5% nonfat dry milk. Anti- β-actin (anti-Actb) antibody (1:3000; GTX637675, GeneTex) was used to control the loading. Proteins were detected using SuperSignal West Femto Maximum Sensitivity Substrate (#34094, ThermoFisher Scientific) and the ImageQuant LAS 4000 (GE Healthcare).

Whole genome bisulfite sequencing (WGBS) and data analysis

Genomic DNA was isolated from retinas using the QIAamp DNA Mini Kit (#51304, Qiagen). The DNA concentration was measured using Qubit 4 Fluorometer and the NanoDrop One spectrophotometer. The quality of genomic DNA was assessed using the Agilent fragment analyzer system. Prior to WGBS library preparation, genomic DNA spiked with unmethylated lambda DNA was fragmented via sonication to produce 350 bp DNA fragments using Covaris S220. To prepare WGBS libraries, we used the EZ DNA Methylation-Gold Kit (D5005, Zymo Research) and xGen™ Methyl-Seq DNA Library Prep Kit (#10009860, Integrated DNA Technologies, Inc.) according to manufacturer's instructions. WGBS libraries were sequenced from both ends using a 2□×□150 paired end (PE) configuration. The FASTQ files obtained in this study were uploaded to the BioProject database (https://www.ncbi.nlm.nih.gov/bioproject/) and are available under the accession number PRJNA1121391. We used bismark aligner, GENCODE M25 (GRCm38.p6) Mus musculus reference (mm10) genome, and a basic workflow to align paired-end reads [39]. To determine the methylation state of cytosines and to compute the percentage of methylation, we used the cytosine2coverage and bismark_methylation_extractor modules of bismark. To get the average X coverage, we used the SAMtools software and our bam files. The results of our calculations indicate that the average base coverage of the genome was 11.4X for TET_1, 9.4X for TET_2, 10.1X for TET_3, 9.2X for Chx10-TET_1, 11.7X for Chx10-TET_2, 15X for Chx10-TET_3. Thus, the total average base coverage of the TET genome was 30.9X, the total average base coverage of the Chx10-TET genome was 35.9X. CpG methylation clustering, CPG methylation PCA analysis, average DNA methylation levels, and identification of genomic region segmentation classes were accomplished using the methylKit R Bioconductor package [20]. Annotation was performed using the annotatr R Bioconductor package [21]. We used ShinyGO (ver. 0.80, http://bioinformatics.sdstate.edu/go/) to identify important signaling cascades and biological processes. The Integrative Genomics Viewer (IGV, https://igv.org/) was used to visualize methylated cytosines.

Statistical Analysis

The unpaired Student's t-test was applied for experiments containing one variable. For experiments containing two or more variables, a one-way analysis of variance (ANOVA) was utilized. P values equal to or less than 0.05 were considered statistically significant. Negative and positive controls were always used in our study. Animal experiments utilized offspring from several different breeding pairs in every experimental group to avoid the potential for a unique genetic bias. Generation and analysis of next-

generation sequencing (NGS) data were carried out in-house according to ENCODE standards and pipelines.

Data availability
The datasets collected and analyzed in this study are available in the BioProject database (accession number PRJNA1121391) and in the article/Supplementary Data. We also used Gene Expression Omnibus (GEO) NCBI GSE101986 and GSE104827 datasets to examine the expression of *Tet1, Tet2*, and *Tet3* genes in developing mouse and human retinas.

Acknowledgments
This study was supported in part by the National Institutes of Health/National Eye Institute, grants R01 EY035235 (D.I.), National Institutes of Health/National Eye Institute Center Core grant P30 EY014801, and Research to Prevent Blindness/ Unrestricted Grant GR004596-1. We are grateful to Dr. Anjana Rao (La Jolla Institute for Immunology) for the animals she provided to us. The authors thank Charles K. Yaros for his expert assistance. We acknowledge the University of Miami Transmission Electron Microscopy Core for EM sample preparation and assistance with the generation of EM images.

Competing interests
The authors declare no competing interests.

Supplementary information
Supplementary Fig. S1. The thickness of the TET and Chx10-TET retinal layers was measured every 200 µm, starting from the head of the optic nerve. The retinal size meant the length of the arc passing from the periphery of the retina on the left through the optic nerve head up to the periphery of the retina on the right.

Supplementary Fig. S2. We found that already in postnatal day 14 (P14) Chx10-TET mice, the thickness of the retinal outer segments (OS) and outer plexiform layers (OPL) measured every 200 µm was significantly less compared to the thickness of the OS and OPL of the TET retinas. The difference in the thickness of the outer nuclear layer (ONL) of the Chx10-TET vs. TET retinas was evident in 1-month-old animals and became significant in 3- and 6-month-old animals. In general, the inner nuclear layers (INL) and inner plexiform layers (IPL) did not differ much in animals of all ages studied. The observed increase in the thickness of the INL of the 6-month-old Chx10-TET retinas is likely due to the fact that their cells move and begin to fill the space previously occupied by the cells of the ONL.

Supplementary Fig. S3. Slow Chx10-TET retinal degeneration occurs because a small number of TET-deficient photoreceptors die over a period of time. **A)** While we did not find TUNEL-positive dead cells in TET retinas, we found only a few TUNEL-positive dead cells in the ONL of Chx10-TET retinas. **B)** Positive controls were treated with DNase I to induce TUNEL-positive DNA strand breaks. (red - TUNEL-positive dead cells, blue - Hoechst 33342-positive cell nuclei)

Supplementary Fig. S4. The TET-dependent DNA demethylation pathway is required for the development of photoreceptor outer segments and synapses. **A)** While the OS of the retinas was fully developed in 1-month-old TET animals, transmission electron microscopy (TEM) examination revealed the absence or underdevelopment of the OS in the retinas of 1-month-old Chx10-TET mice. However, due to the mosaic nature of cre recombinase expression in Chx10-cre mice, it was sometimes possible to find relatively well-developed OS in certain areas of the retinas of Chx10-TET animals. **B)** The retinal ONL and INL of 1-month-old TET animals were separated by OPL in which many well-developed synapses (s, B') were identified. The OPL and the synapses in it were difficult to detect in the retinas of 1-month-old Chx10-TET animals (B''). The lack of a barrier between the ONL and INL leads to mixing of their cells in Chx10-TET retinas. However, due to the mosaic nature of cre recombinase expression, it

was possible to find areas where synapses were well developed in Chx10-TET animals (B'''). We collected retinas from five 1-month-old TET and Chx10-TET mice for TEM analysis. All images were collected at the same distance from the optic nerve head (800 µm). The dark blue stars limit the layer that contains retinal pigment epithelial (RPE) cells. Red stars indicate the boundary of the outer nuclear layer (ONL). Blue stars indicate the boundary of the inner nuclear layer (INL).

Supplementary Fig. S5. One-month-old Chx10-TET mice were functionally blind as indicated by ERG tests. **A)** Scotopic ERGs: both eyes of dark-adapted animals were subjected to an intensity series of single white-light flash stimulus at 0.01, 0.1, and 1.0 cd.s/m^2 at a frequency of 1.00 Hz. B-wave amplitudes (derived primarily from Muller cells and ON-bipolar cells) were analyzed as the amplitude from the trough of the a-wave to the peak to the subsequent b-wave peak. The negative trough of the a-wave (derived from photoreceptors, rods and cones) was analyzed at 1.0 cd.s/m^2 intensity. **B)** Photopic ERGs: light-adapted animals were presented with a 3 and 10 cd.s/m2 flash intensity ERG. **C)** Flicker ERG: measures cone opsin regeneration rate. Animals were exposed to continuous 6500K white light flash cycles at an intensity of 3 cd.s/m^2 with frequencies of 10 or 30 Hz, against a background of 30 cd/m^2 6500K white light. Flicker amplitudes were measured from the N1 trough to the subsequent P1 peak. **D)** Oscillatory potentials (primarily from amacrine cells) were automatically isolated and measured from the ascending limb of the b-wave by the Epsion software (V6.64.14; Diagnosys LLC) at 1 cd.s/m^2. Representative traces are shown. For all tests n=14 eyes (7 animals per group, TET or Chx10-TET) were sampled. For all tests an unpaired t-test was performed between the two groups and was significant to P value <0.0001 (****).

Supplementary Fig. S6. Genetic ablation of the TET family in RPCs results in a significant reduction in the expression of transcripts encoding Tet1, Tet2, and Tet3 catalytic domains in the adult retina. **(A-F)** Visualization of the RNA-seq data using Integrative Genomics Viewer (IGV) revealed low read content in exons encoding catalytic domains of *Tet1* (**A, B**), *Tet2* (**C, D**), and *Tet3* (**E, F**) in Chx10-TET vs. TET mice. **G)** The expression of *Tet1, Tet2*, and *Tet3*, considering transcripts with and without catalytic domains, does not differ in Chx10-TET and TET retinas. **(H, I)** If we only take into account reads corresponding to exons encoding Tet1 (Tet1ex10_12), Tet2 (Tet2ex8_10), and Tet3 (Tet2ex3) catalytic domains, then the expression of transcripts encoding catalytic domains is significantly reduced in the retinas of P14 (**H**) and 1-month-old (**I**) Chx10-TET mice. These results indicate the stability of *Tet1, Tet2*, and *Tet3* transcripts that do not contain exons encoding catalytic domains.

Supplementary Fig. S7. Visualization of individual methylated and unmethylated cytosines in gene promoters indicate a high content of methylated cytosines near the transcription start site (TSS) in DNA isolated from the retinas of P14 Chx10-TET mice. At the same time, cytosines located at the same positions were low methylated (hypomethylated) in DNA isolated from P14 TET mouse retinas. The figure shows the promoters of the following genes: *Nr2e3* (**A, B**), *Pde6a* (**C, D**), *Rho* (**R, F**), *Pde6b* (**G, H**), *Prph2* (**I, J**), and *Rcvrn* (**K, L**). We used Integrative Genomics Viewer (IGV) to visualize the bed files (% of C methylation in CpG context) that were generated by Bismark Bisulfite Mapper.

Supplementary Data S1. The results of the RNA-seq analysis indicate that the expression of many genes necessary for the development of the photoreceptor outer segment, inner segment, cell cilium, and synapses, as well as the expression of many genes necessary for phototransduction, was significantly reduced in the retinas of P14 and 1-month-old Chx10-TET compared to TET mice. Many of these genes have been implicated in various forms of retinitis pigmentosa, cone and cone-rod dystrophy, congenital stationary night blindness, and Leber congenital amaurosis.

Supplementary Data S2. The combination of methylKit and annotatr Bioconductor R packages made it possible to determine the average level of methylation of promoters and first exons of genes. A search for genes whose promoters and first exons were highly methylated (hypermethylated) in DNA isolated from

P14 Chx10-TET retinas compared to P14 TET retinas resulted in a list of genes, many of which are essential for photoreceptor development and function.

Figure legends

Fig. 1. The TET-dependent DNA demethylation pathway is required for photoreceptor development and function. **(A, B)** The RNA-seq data from NCBI (GSE101986 and GSE104827 datasets) indicate that members of the TET family and *Vsx2* (Chx10) gene are expressed at all stages of human (**A**) and mouse (**B**) retinal development, including the earliest stages when the retina is predominantly composed of RPCs (embryonic day (E) 11.5 in mice and human gestation days 50-60). **C)** The catalytic domains of the Tet1 and Tet2 are encoded by multiple exons, while the catalytic domain of Tet3 is encoded by only one exon. **D)** To inactivate the DNA demethylation pathway, we generated floxed TET mice in which the catalytic domains of all genes of the TET family were flanked by loxP sites. To inactivate this pathway directly in RPCs, we crossed TET with Chx10-cre to get Chx10-TET mice. **E)** The sizes of the eyeballs of 3-month-old Chx10-TET mice were smaller than those of TET and Chx10-cre mice of the same age (n=6-8 eyes per group; apd – anterior-posterior diameter, h/vd – horizontal/vertical diameter). **F)** While the retinas of 3-month-old TET and Chx10-cre mice were normally developed, the photoreceptor outer segments (OS) and the outer plexiform layer (OPL) were virtually undetectable in 3-month-old mice. In the absence of the OPL, the cells of the outer nuclear layer (ONL) and the inner nuclear layer (INL) were intermingled. **(G-I)** ERG potentials recorded from dark-adapted (rod) and light-adapted (cone) animals indicates that Chx10-TET mice were functionally blind. Dark-adapted (**G**) animals were subjected to a white-light flash stimulus at an intensity of 1.0 cd.s/m^2 and frequency of 1.00 Hz. B-wave amplitudes were analyzed as the amplitude from the trough of the a-wave to the peak to the subsequent b-wave peak. The negative trough of the a-wave was analyzed at 1.0 cd.s/m^2 intensity. Light-adapted (**H**) animals were presented with a 10 cd.s/m^2 flash intensity ERG. Animal eyes were exposed to white light flash cycles at an intensity of 3 cd.s/m^2 with frequencies of 10 Hz, against a background of 30 cd.s/m^2 white light (**I**). Flicker amplitudes were measured from the N1 trough to the subsequent P1 peak. (n=10-20 eyes or 5-10 mice per group; P value <0.0001 [****], P value <0.001 [***], P value <0.01 [**])

Fig. 2. The impaired activity of the TET-dependent DNA demethylation pathway in RPCs leads to the formation of photoreceptors without OS and synaptic termini, which ends in their slow death. **A)** The representative confocal images show retinal morphology and the change in this morphology over time in TET and Chx10-TET mice (PNA is a marker of cone OS, Rho is a marker of rod OS). **B)** The results of an analysis of the thickness of the retinal layers indicate a slow degeneration of photoreceptors leading to retinal dystrophy in Chx10-TET animals. TET-deficient retinas are also smaller in size compared to TET retinas. (n=5 mice per group, per age; P value <0.0001 [****], P value <0.001 [***]) **(C-E)** TEM examination of 1-month-old animals indicates underdevelopment or absence of OS **(C)** and synapses **(s, D-D”)** in TET-deficient photoreceptors. The small number of synapses in the outer plexiform layer (OPL) leads to the fact that cells of the outer nuclear layer (ONL) and the inner nuclear layer (INL) can mix freely in Chx10-TET retinas **(D)**. Chromatin is less condensed in the nuclei of TET-deficient photoreceptors located in the ONL **(E)**. All images were collected at the same distance from the optic nerve head (800 µm). The dark blue stars limit the layer that contains retinal pigment epithelial (RPE) cells. Red stars indicate the boundary of the ONL. Blue stars indicate the boundary of the INL. n=5 retinas or 5 mice per group

Fig. 3. The TET-dependent DNA demethylation pathway has less influence on the differentiation of non-photoreceptors from RPCs. **(A, B)** While s-opsin (Opn1sw is a marker of blue cones) can still be detected in the retinas of 3-month-old Chx10-TET mice **(A)**, m-opsin (Opn1mw **[A]** is a marker of green cones) and rhodopsin (Rho **[B]** is a marker of rods) are absent in the retinas of Chx10-TET mice. **C)** Rcvrn, as a marker of photoreceptors and bipolar cells, was less expressed in the Chx10-TET retinas. However, bipolar cells (Chx10 as a marker) were present in the retinas of Chx10-TET animals. **(D, E)** Muller glia

(Glul as a marker) was less organized in the retinas of 3-month-old Chx10-TET mice **(D)**. The expression of the marker of these cells was reduced as follows from the western blot. **F)** Horizontal cells (Calbindin D as a marker) and amacrine cells (ChAT as a marker) were present in Chx10-TET retinas. However, synaptic contacts were disorganized **(F', F")** in the retinal IPL of Chx10-TET animals. **(G, H)** The thickness of the optic nerves was significantly less in 3-month-old Chx10-TET than in TET mice (n=10-12 optic nerves or 5-6 mice per group; P value <0.0001 [****]). At the same time, RGC (Rbpms and Tubb3 as markers) density in the ganglion cell layer (GCL) did not differ between Chx10-TET and TET mice.

Fig. 4. The activity of the TET-dependent DNA demethylation pathway is necessary for the expression of genes responsible for rod specification and for rod and cone maturation. **(A-C)** The sample clustering **(A)**, principal component analysis (PCA, **B**), and volcano plots **(C)** indicate that RNA-seq data collected from the retinas of P14 (p) and 1-month-old (m) Chx10-TET mice differ significantly from RNA-seq data collected from the retinas of TET mice of the same ages. **D)** K-means clustering revealed six distinctive clusters. Cluster six, in which gene expression is significantly reduced in Chx10-TET vs. TET retinas, contains predominantly genes necessary for the development and function of photoreceptors. **(E, F)** The figure **(E)** shows the percentages of genes with decreased (green), increased (orange), and unchanged (dark blue) expression depending on the function they perform in photoreceptors. Many genes whose expression was reduced are responsible for the specification and maturation of rods (**F**, purple). The expression of many genes responsible for cone maturation is increased (**F**, blue). The expression of genes necessary for rod and cone maturation is decreased (**F**, black). **G)** Mutations in many genes whose expression has been reduced (green) in Chx10-TET vs. TET retinas lead to various types of retinal dystrophies. **H)** The reduced expression of *Nr2e3*, *Pde6b*, *Prph2*, *Rho*, and *Rcvrn* genes is consistent with the low levels of the proteins they encode in the retinas of the Chx10-TET animals, as follows from the western blot analysis. Anti- β-actin (anti-Actb) antibody was used to control the loading.

Fig. 5. Disruption of the TET-dependent DNA demethylation pathway prevents demethylation of the promoters of genes essential for photoreceptor development and function. **(A, B)** The CpG methylation clustering **(A)** and principal component analysis **(B)** indicate that DNA isolated from retinas of P14 Chx10-TET mice has a methylation pattern that is significantly different from that of DNA isolated from retinas of P14 TET mice. (**C, D**) The results of the analysis of genes whose promoters remain highly methylated in Chx10-TET retinas but are demethylated in TET retinas indicate their predominant association with the development **(C)**, function **(C)**, and pathology **(D)** of photoreceptors. **E)** The figure shows the relationship between the level of promoter methylation and the expression of the corresponding genes. **F)** Visualization of the average % CpG methylation corresponding to different DNA regions indicates that the promoters of genes important for the development and function of photoreceptors were highly methylated (hypermethylated) in Chx10-TET retinas and low methylated (hypomethylated) in TET retinas. We used Integrative Genomics Viewer (IGV) to visualize the bed files that were generated by Bismark Bisulfite Mapper.

References

1. Molday, R.S. & Moritz, O.L. Photoreceptors at a glance. *J Cell Sci* **128**, 4039-4045 (2015).
2. Baden, T., Euler, T. & Berens, P. Understanding the retinal basis of vision across species. *Nat Rev Neurosci* **21**, 5-20 (2020).
3. Swaroop, A., Kim, D. & Forrest, D. Transcriptional regulation of photoreceptor development and homeostasis in the mammalian retina. *Nat Rev Neurosci* **11**, 563-576 (2010).
4. Cepko, C.L. The Determination of Rod and Cone Photoreceptor Fate. *Annu Rev Vis Sci* **1**, 211-234 (2015).
5. Georgiou, M., *et al.* Phenotyping and genotyping inherited retinal diseases: Molecular genetics, clinical and imaging features, and therapeutics of macular dystrophies, cone and cone-rod dystrophies,

rod-cone dystrophies, Leber congenital amaurosis, and cone dysfunction syndromes. *Prog Retin Eye Res* **100**, 101244 (2024).
6. Broadgate, S., Yu, J., Downes, S.M. & Halford, S. Unravelling the genetics of inherited retinal dystrophies: Past, present and future. *Prog Retin Eye Res* **59**, 53-96 (2017).
7. Hartong, D.T., Berson, E.L. & Dryja, T.P. Retinitis pigmentosa. *Lancet* **368**, 1795-1809 (2006).
8. Du, J., Johnson, L.M., Jacobsen, S.E. & Patel, D.J. DNA methylation pathways and their crosstalk with histone methylation. *Nature reviews. Molecular cell biology* **16**, 519-532 (2015).
9. Corso-Diaz, X., Jaeger, C., Chaitankar, V. & Swaroop, A. Epigenetic control of gene regulation during development and disease: A view from the retina. *Prog Retin Eye Res* **65**, 1-27 (2018).
10. Wu, X. & Zhang, Y. TET-mediated active DNA demethylation: mechanism, function and beyond. *Nat Rev Genet* **18**, 517-534 (2017).
11. Pastor, W.A., Aravind, L. & Rao, A. TETonic shift: biological roles of TET proteins in DNA demethylation and transcription. *Nature reviews. Molecular cell biology* **14**, 341-356 (2013).
12. Dvoriantchikova, G., Lypka, K.R. & Ivanov, D. The Potential Role of Epigenetic Mechanisms in the Development of Retinitis Pigmentosa and Related Photoreceptor Dystrophies. *Front Genet* **13**, 827274 (2022).
13. Dvoriantchikova, G., Seemungal, R.J. & Ivanov, D. DNA Methylation Dynamics During The Differentiation Of Retinal Progenitor Cells Into Retinal Neurons Reveal A Role For The DNA Demethylation Pathway. *Front. Mol. Neurosci.* **12** (2019).
14. Kim, J.W., *et al.* NRL-Regulated Transcriptome Dynamics of Developing Rod Photoreceptors. *Cell Rep* **17**, 2460-2473 (2016).
15. Hoshino, A., *et al.* Molecular Anatomy of the Developing Human Retina. *Dev Cell* **43**, 763-779 e764 (2017).
16. Kang, J., *et al.* Simultaneous deletion of the methylcytosine oxidases Tet1 and Tet3 increases transcriptome variability in early embryogenesis. *Proc Natl Acad Sci U S A* **112**, E4236-4245 (2015).
17. Ko, M., *et al.* Ten-Eleven-Translocation 2 (TET2) negatively regulates homeostasis and differentiation of hematopoietic stem cells in mice. *Proc Natl Acad Sci U S A* **108**, 14566-14571 (2011).
18. Rowan, S. & Cepko, C.L. Genetic analysis of the homeodomain transcription factor Chx10 in the retina using a novel multifunctional BAC transgenic mouse reporter. *Dev Biol* **271**, 388-402 (2004).
19. Jeon, C.J., Strettoi, E. & Masland, R.H. The major cell populations of the mouse retina. *J Neurosci* **18**, 8936-8946 (1998).
20. Akalin, A., *et al.* methylKit: a comprehensive R package for the analysis of genome-wide DNA methylation profiles. *Genome Biol* **13**, R87 (2012).
21. Cavalcante, R.G. & Sartor, M.A. annotatr: genomic regions in context. *Bioinformatics* **33**, 2381-2383 (2017).
22. Sapkota, D., *et al.* Onecut1 and Onecut2 redundantly regulate early retinal cell fates during development. *Proc Natl Acad Sci U S A* **111**, E4086-4095 (2014).
23. Emerson, M.M., Surzenko, N., Goetz, J.J., Trimarchi, J. & Cepko, C.L. Otx2 and Onecut1 promote the fates of cone photoreceptors and horizontal cells and repress rod photoreceptors. *Dev Cell* **26**, 59-72 (2013).
24. Ivanov, D. Notch Signaling-Induced Oscillatory Gene Expression May Drive Neurogenesis in the Developing Retina. *Front Mol Neurosci* **12**, 226 (2019).
25. Dawlaty, M.M., *et al.* Loss of Tet enzymes compromises proper differentiation of embryonic stem cells. *Dev Cell* **29**, 102-111 (2014).
26. Sun, Z., *et al.* EGR1 recruits TET1 to shape the brain methylome during development and upon neuronal activity. *Nat Commun* **10**, 3892 (2019).
27. Li, X., *et al.* Ten-eleven translocation 2 interacts with forkhead box O3 and regulates adult neurogenesis. *Nat Commun* **8**, 15903 (2017).
28. Costa, Y., *et al.* NANOG-dependent function of TET1 and TET2 in establishment of pluripotency. *Nature* **495**, 370-374 (2013).

29. Okashita, N., *et al.* PRDM14 promotes active DNA demethylation through the ten-eleven translocation (TET)-mediated base excision repair pathway in embryonic stem cells. *Development* **141**, 269-280 (2014).
30. Wang, Y., *et al.* WT1 recruits TET2 to regulate its target gene expression and suppress leukemia cell proliferation. *Mol Cell* **57**, 662-673 (2015).
31. Perera, A., *et al.* TET3 is recruited by REST for context-specific hydroxymethylation and induction of gene expression. *Cell Rep* **11**, 283-294 (2015).
32. Fujiki, K., *et al.* PPARgamma-induced PARylation promotes local DNA demethylation by production of 5-hydroxymethylcytosine. *Nat Commun* **4**, 2262 (2013).
33. Ait-Ali, N., *et al.* Rod-derived cone viability factor promotes cone survival by stimulating aerobic glycolysis. *Cell* **161**, 817-832 (2015).
34. Dobin, A., *et al.* STAR: ultrafast universal RNA-seq aligner. *Bioinformatics* **29**, 15-21 (2013).
35. Putri, G.H., Anders, S., Pyl, P.T., Pimanda, J.E. & Zanini, F. Analysing high-throughput sequencing data in Python with HTSeq 2.0. *Bioinformatics* (2022).
36. Robinson, M.D., McCarthy, D.J. & Smyth, G.K. edgeR: a Bioconductor package for differential expression analysis of digital gene expression data. *Bioinformatics* **26**, 139-140 (2010).
37. Love, M.I., Huber, W. & Anders, S. Moderated estimation of fold change and dispersion for RNA-seq data with DESeq2. *Genome Biol* **15**, 550 (2014).
38. Ge, S.X., Son, E.W. & Yao, R. iDEP: an integrated web application for differential expression and pathway analysis of RNA-Seq data. *BMC Bioinformatics* **19**, 534 (2018).
39. Krueger, F. & Andrews, S.R. Bismark: a flexible aligner and methylation caller for Bisulfite-Seq applications. *Bioinformatics* **27**, 1571-1572 (2011).

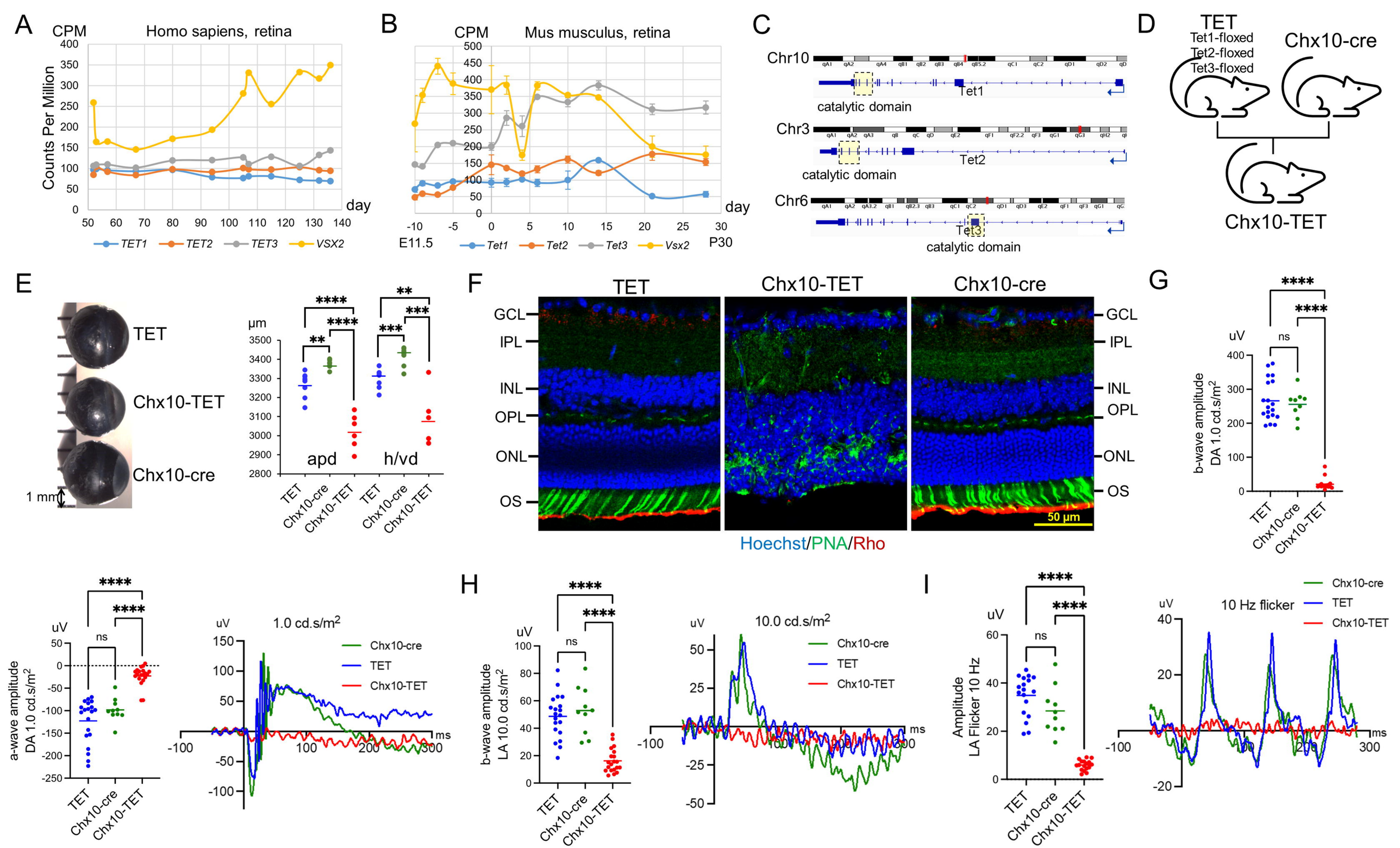
A
CPM
Homo sapiens, retina
Counts Per Million
day
TET1
TET2
TET3
VSX2
B
CPM
Mus musculus, retina
day
E11.5
P30
Tet1
Tet2
Tet3
Vsx2
C
Chr10
Tet1
catalytic domain
Chr3
Tet2
catalytic domain
Chr6
Tet3
catalytic domain
D
TET
Tet1-floxed
Tet2-floxed
Tet3-floxed
Chx10-cre
Chx10-TET
E
TET
Chx10-TET
Chx10-cre
1 mm
µm
apd
h/vd
TET
Chx10-cre
Chx10-TET
F
TET
Chx10-TET
Chx10-cre
GCL
IPL
INL
OPL
ONL
OS
50 µm
Hoechst/PNA/Rho
G
uV
ns
b-wave amplitude
DA 1.0 cd.s/m²
TET
Chx10-cre
Chx10-TET
a-wave amplitude
DA 1.0 cd.s/m²
1.0 cd.s/m²
ms
H
b-wave amplitude
LA 10.0 cd.s/m²
10.0 cd.s/m²
I
Amplitude
LA Flicker 10 Hz
10 Hz flicker

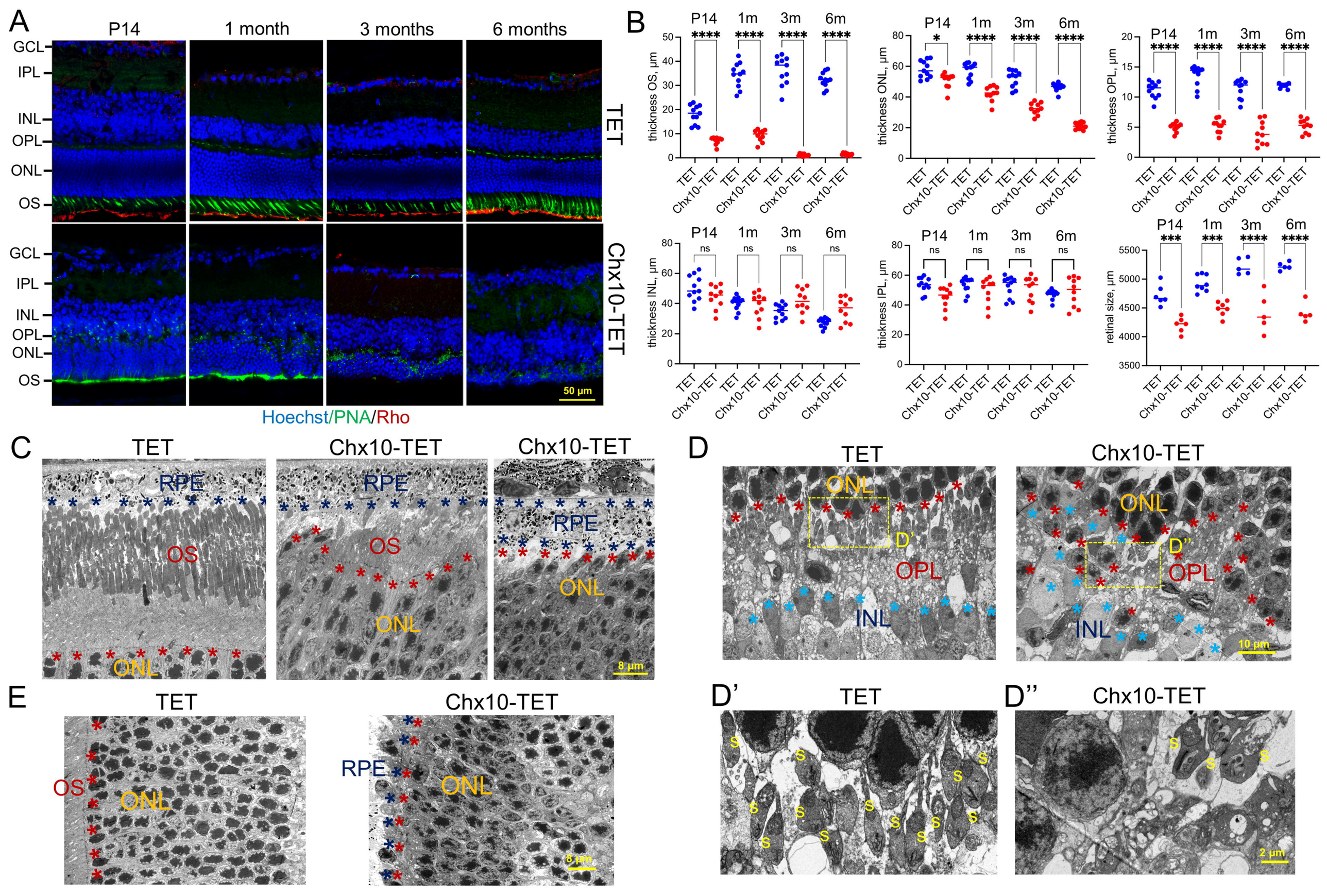
A
P14
1 month
3 months
6 months
GCL
IPL
INL
OPL
ONL
OS
TET
Chx10-TET
50 µm
Hoechst/PNA/Rho
B
P14
1m
3m
6m
thickness OS, µm
thickness ONL, µm
thickness OPL, µm
thickness INL, µm
thickness IPL, µm
retinal size, µm
TET
Chx10-TET
ns
C
TET
Chx10-TET
RPE
OS
ONL
8 µm
D
D'
D''
OPL
INL
10 µm
E
S
2 µm

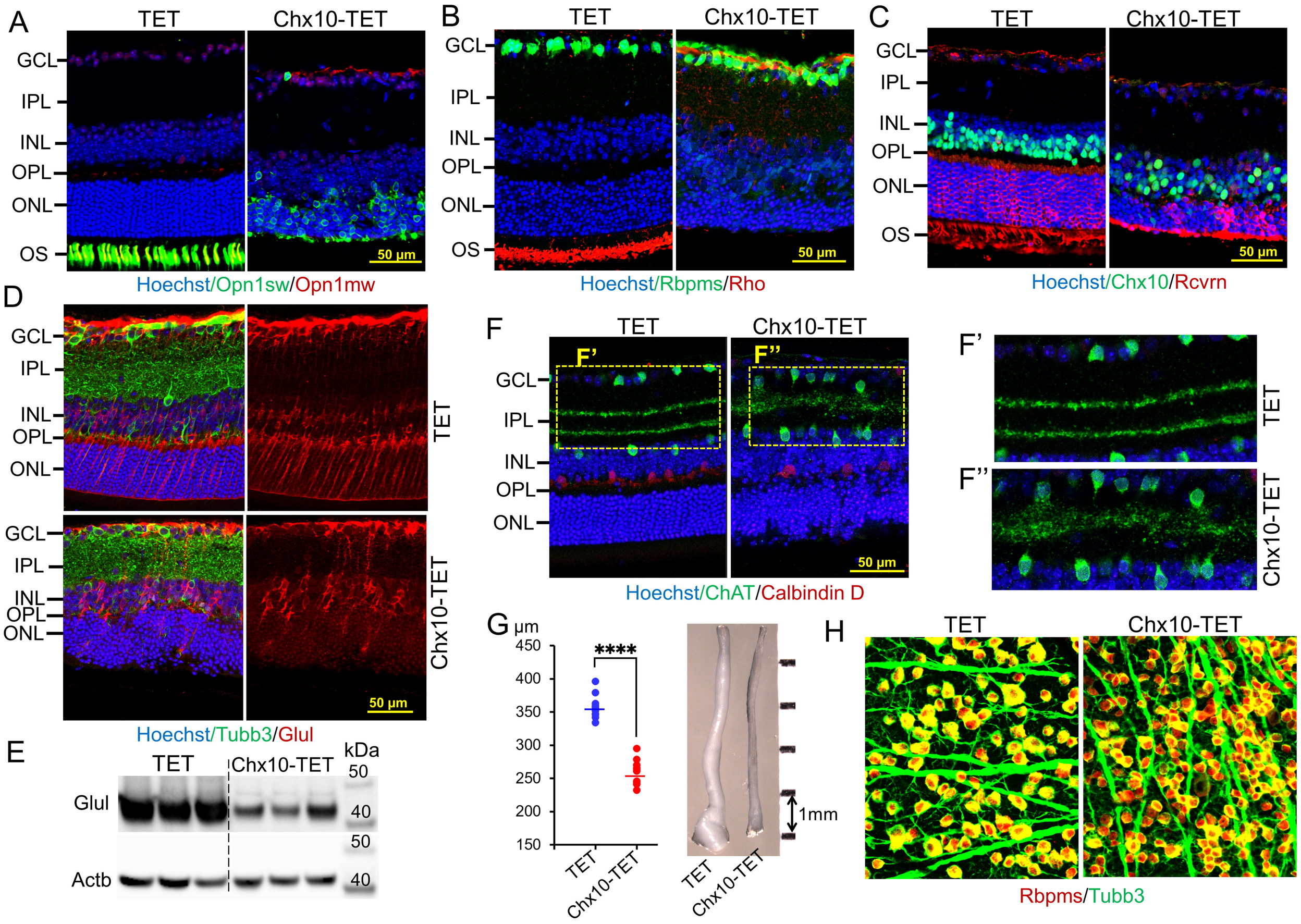
A
TET
Chx10-TET
GCL
IPL
INL
OPL
ONL
OS
50 µm
Hoechst/Opn1sw/Opn1mw
B
TET
Chx10-TET
GCL
IPL
INL
OPL
ONL
OS
50 µm
Hoechst/Rbpms/Rho
C
TET
Chx10-TET
GCL
IPL
INL
OPL
ONL
OS
50 µm
Hoechst/Chx10/Rcvrn
D
GCL
IPL
INL
OPL
ONL
TET
GCL
IPL
INL
OPL
ONL
Chx10-TET
50 µm
Hoechst/Tubb3/Glul
E
TET
Chx10-TET
kDa
Glul
50
40
Actb
50
40
F
TET
Chx10-TET
F'
F''
GCL
IPL
INL
OPL
ONL
50 µm
Hoechst/ChAT/Calbindin D
F'
TET
F''
Chx10-TET
G
µm
450
400
350
300
250
200
150
****
TET
Chx10-TET
1mm
H
TET
Chx10-TET
Rbpms/Tubb3

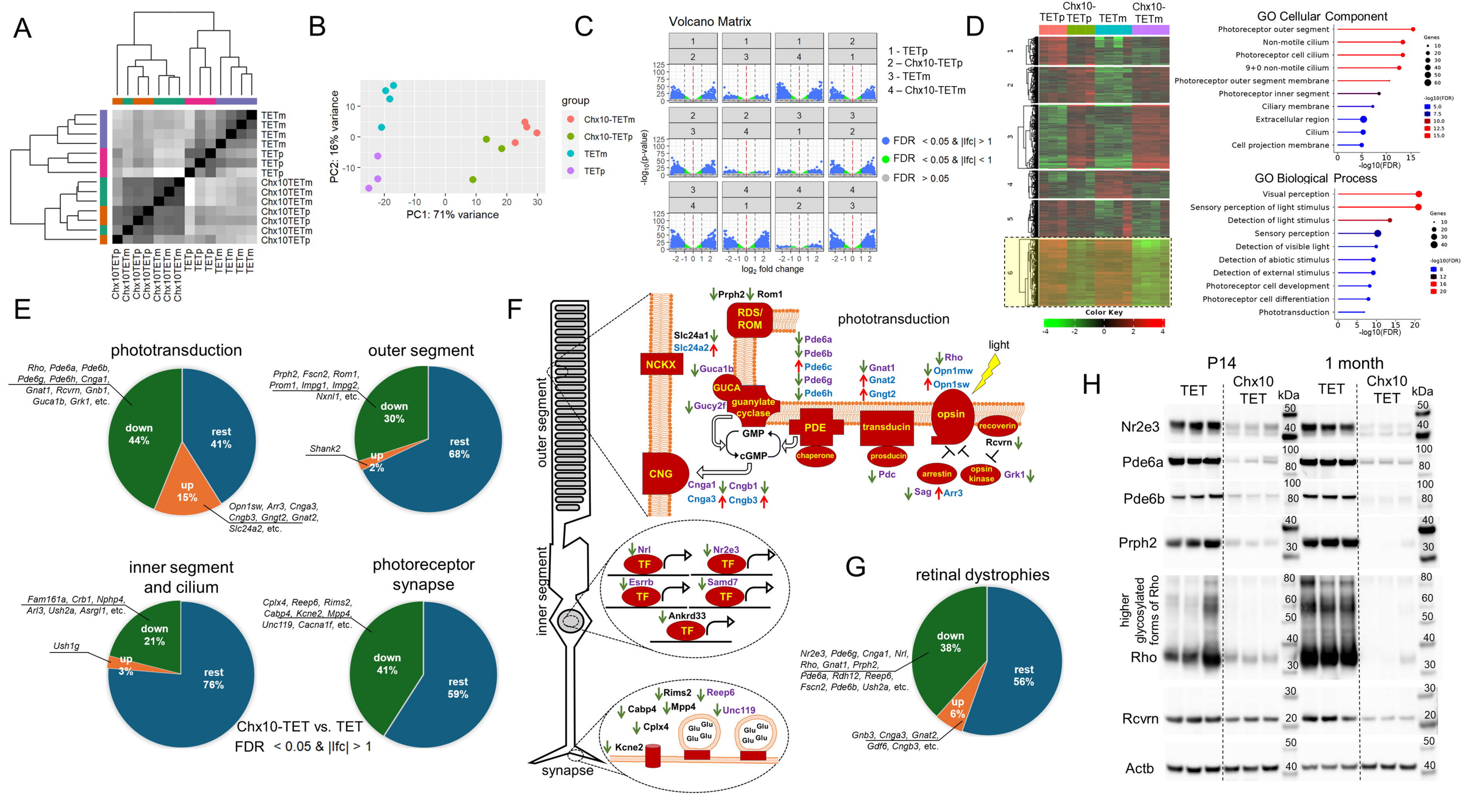
A
TETm
TETp
Chx10TETm
Chx10TETp
B
PC2: 16% variance
PC1: 71% variance
group
Chx10-TETm
Chx10-TETp
TETm
TETp
C
Volcano Matrix
1 - TETp
2 – Chx10-TETp
3 - TETm
4 – Chx10-TETm
FDR < 0.05 & |lfc| > 1
FDR < 0.05 & |lfc| < 1
FDR > 0.05
-log10(p-value)
log2 fold change
D
TETp
Chx10-TETp
TETm
Chx10-TETm
Color Key
GO Cellular Component
Photoreceptor outer segment
Non-motile cilium
Photoreceptor cell cilium
9+0 non-motile cilium
Photoreceptor outer segment membrane
Photoreceptor inner segment
Ciliary membrane
Extracellular region
Cilium
Cell projection membrane
-log10(FDR)
GO Biological Process
Visual perception
Sensory perception of light stimulus
Detection of light stimulus
Sensory perception
Detection of visible light
Detection of abiotic stimulus
Detection of external stimulus
Photoreceptor cell development
Photoreceptor cell differentiation
Phototransduction
E
phototransduction
Rho, Pde6a, Pde6b, Pde6g, Pde6h, Cnga1, Gnat1, Rcvrn, Gnb1, Guca1b, Grk1, etc.
down 44%
rest 41%
up 15%
Opn1sw, Arr3, Cnga3, Cngb3, Gngt2, Gnat2, Slc24a2, etc.
outer segment
Prph2, Fscn2, Rom1, Prom1, Impg1, Impg2, Nxnl1, etc.
down 30%
Shank2
up 2%
rest 68%
inner segment and cilium
Fam161a, Crb1, Nphp4, Arl3, Ush2a, Asrgl1, etc.
down 21%
Ush1g
up 3%
rest 76%
photoreceptor synapse
Cplx4, Reep6, Rims2, Cabp4, Kcne2, Mpp4, Unc119, Cacna1f, etc.
down 41%
rest 59%
Chx10-TET vs. TET
FDR < 0.05 & |lfc| > 1
F
outer segment
inner segment
synapse
phototransduction
Prph2
Rom1
RDS/ ROM
Slc24a1
Slc24a2
NCKX
Guca1b
GUCA
guanylate cyclase
Gucy2f
Pde6a
Pde6b
Pde6c
Pde6g
Pde6h
PDE
chaperone
GMP
cGMP
CNG
Cnga1
Cngb1
Cnga3
Cngb3
Gnat1
Gnat2
Gngt2
transducin
prosducin
Pdc
Rho
Opn1mw
Opn1sw
light
opsin
recoverin
Rcvrn
arrestin
opsin kinase
Grk1
Sag
Arr3
Nrl
TF
Nr2e3
Esrrb
Samd7
Ankrd33
Rims2
Reep6
Cabp4
Mpp4
Unc119
Cplx4
Kcne2
Glu
G
retinal dystrophies
down 38%
rest 56%
up 6%
Nr2e3, Pde6g, Cnga1, Nrl, Rho, Gnat1, Prph2, Pde6a, Rdh12, Reep6, Fscn2, Pde6b, Ush2a, etc.
Gnb3, Cnga3, Gnat2, Gdf6, Cngb3, etc.
H
P14
1 month
TET
Chx10 TET
kDa
Nr2e3
Pde6a
Pde6b
Prph2
higher glycosylated forms of Rho
Rho
Rcvrn
Actb

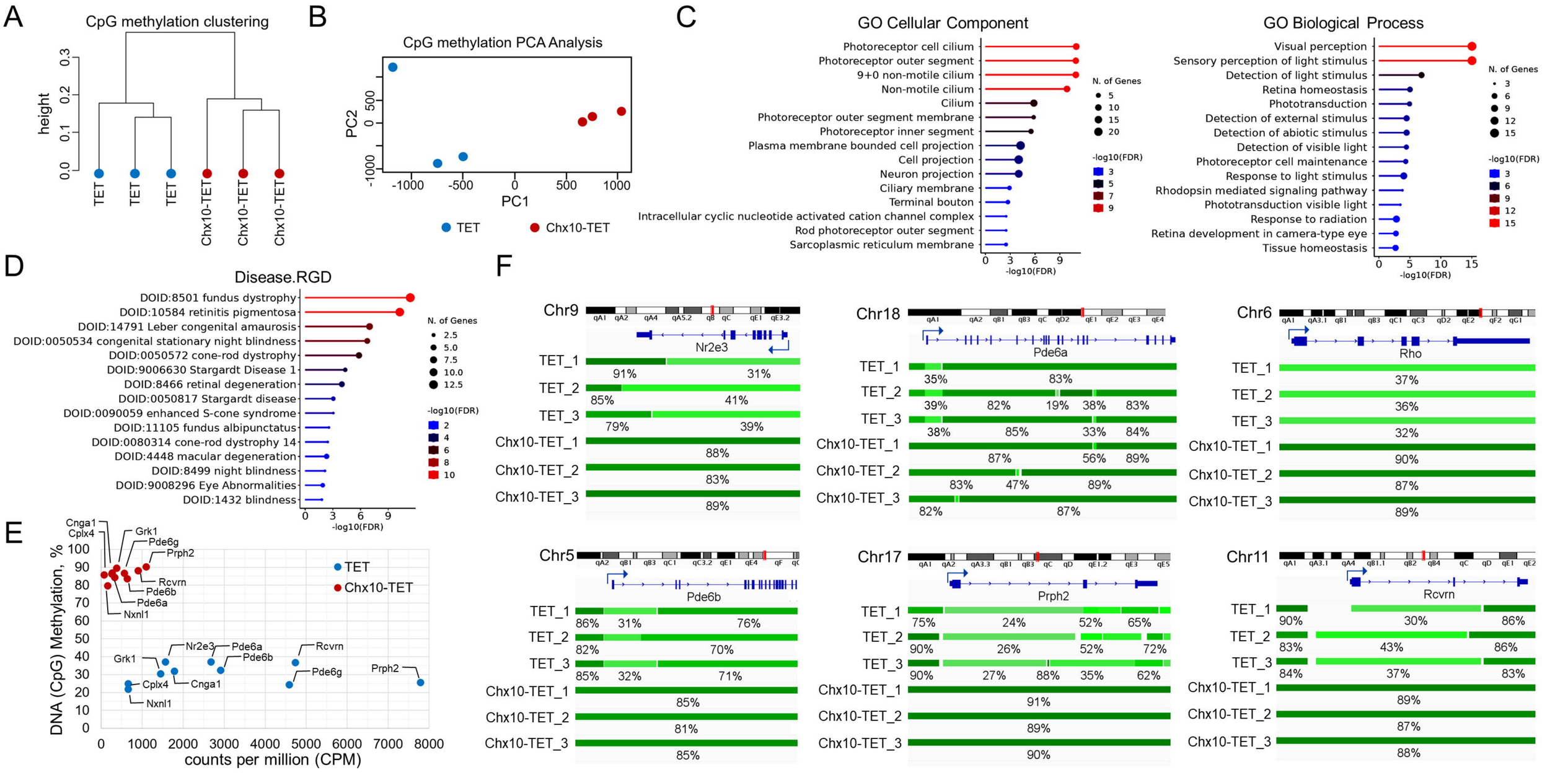
A
CpG methylation clustering
height
0.0
0.1
0.2
0.3
TET
TET
TET
Chx10-TET
Chx10-TET
Chx10-TET
B
CpG methylation PCA Analysis
PC2
PC1
-1000
-500
0
500
1000
TET
Chx10-TET
C
GO Cellular Component
Photoreceptor cell cilium
Photoreceptor outer segment
9+0 non-motile cilium
Non-motile cilium
Cilium
Photoreceptor outer segment membrane
Photoreceptor inner segment
Plasma membrane bounded cell projection
Cell projection
Neuron projection
Ciliary membrane
Terminal bouton
Intracellular cyclic nucleotide activated cation channel complex
Rod photoreceptor outer segment
Sarcoplasmic reticulum membrane
-log10(FDR)
N. of Genes
5
10
15
20
-log10(FDR)
3
5
7
9
GO Biological Process
Visual perception
Sensory perception of light stimulus
Detection of light stimulus
Retina homeostasis
Phototransduction
Detection of external stimulus
Detection of abiotic stimulus
Detection of visible light
Photoreceptor cell maintenance
Response to light stimulus
Rhodopsin mediated signaling pathway
Phototransduction visible light
Response to radiation
Retina development in camera-type eye
Tissue homeostasis
-log10(FDR)
N. of Genes
3
6
9
12
15
-log10(FDR)
3
6
9
12
15
D
Disease.RGD
DOID:8501 fundus dystrophy
DOID:10584 retinitis pigmentosa
DOID:14791 Leber congenital amaurosis
DOID:0050534 congenital stationary night blindness
DOID:0050572 cone-rod dystrophy
DOID:9006630 Stargardt Disease 1
DOID:8466 retinal degeneration
DOID:0050817 Stargardt disease
DOID:0090059 enhanced S-cone syndrome
DOID:11105 fundus albipunctatus
DOID:0080314 cone-rod dystrophy 14
DOID:4448 macular degeneration
DOID:8499 night blindness
DOID:9008296 Eye Abnormalities
DOID:1432 blindness
-log10(FDR)
N. of Genes
2.5
5.0
7.5
10.0
12.5
-log10(FDR)
2
4
6
8
10
E
DNA (CpG) Methylation, %
counts per million (CPM)
TET
Chx10-TET
Cnga1
Cplx4
Grk1
Pde6g
Prph2
Rcvrn
Pde6b
Pde6a
Nxnl1
Nr2e3
F
Chr9
Nr2e3
TET_1 91% 31%
TET_2 85% 41%
TET_3 79% 39%
Chx10-TET_1 88%
Chx10-TET_2 83%
Chx10-TET_3 89%
Chr18
Pde6a
TET_1 35% 83%
TET_2 39% 82% 19% 38% 83%
TET_3 38% 85% 33% 84%
Chx10-TET_1 87% 56% 89%
Chx10-TET_2 83% 47% 89%
Chx10-TET_3 82% 87%
Chr6
Rho
TET_1 37%
TET_2 36%
TET_3 32%
Chx10-TET_1 90%
Chx10-TET_2 87%
Chx10-TET_3 89%
Chr5
Pde6b
TET_1 86% 31% 76%
TET_2 82% 70%
TET_3 85% 32% 71%
Chx10-TET_1 85%
Chx10-TET_2 81%
Chx10-TET_3 85%
Chr17
Prph2
TET_1 75% 24% 52% 65%
TET_2 90% 26% 52% 72%
TET_3 90% 27% 88% 35% 62%
Chx10-TET_1 91%
Chx10-TET_2 89%
Chx10-TET_3 90%
Chr11
Rcvrn
TET_1 90% 30% 86%
TET_2 83% 43% 86%
TET_3 84% 37% 83%
Chx10-TET_1 89%
Chx10-TET_2 87%
Chx10-TET_3 88%